EVA3D: COMPOSITIONAL 3D HUMAN GENERATION FROM 2D IMAGE COLLECTIONS

Anonymous authors
Paper under double-blind review

Figure 1: EVA3D generates high-quality and diverse 3D humans with photo-realistic RGB renderings and detailed geometry. Only 2D image collections are used for training.

ABSTRACT

Inverse graphics aims to recover 3D models from 2D observations. Utilizing differentiable rendering, recent 3D-aware generative models have shown impressive results of rigid object generation using 2D images. However, it remains challenging to generate articulated objects, like human bodies, due to their complexity and diversity in poses and appearances. In this work, we propose, **EVA3D**, an unconditional 3D human generative model learned from 2D image collections only. EVA3D can sample 3D humans with detailed geometry and render high-quality images (up to 512×256) without bells and whistles (*e.g.* super resolution). At the core of EVA3D is a compositional human NeRF representation, which divides the human body into local parts. Each part is represented by an individual volume. This compositional representation enables **1)** inherent human priors, **2)** adaptive allocation of network parameters, **3)** efficient training and rendering. Moreover, to accommodate for the characteristics of sparse 2D human image collections (*e.g.* imbalanced pose distribution), we propose a pose-guided sampling strategy for better GAN learning. Extensive experiments validate that EVA3D achieves state-of-the-art 3D human generation performance regarding both geometry and texture quality. Notably, EVA3D demonstrates great potential and scalability to "inverse-graphics" diverse human bodies with a clean framework.

1 INTRODUCTION

Inverse graphics studies inverse-engineering of projection physics, which aims to recover the 3D world from 2D observations. It is not only a long-standing scientific quest, but also enables numerous applications in VR/AR and VFX. Recently, 3D-aware generative models (Chan et al., 2021;

Or-El et al., 2022; Chan et al., 2022; Deng et al., 2022) demonstrate great potential in inverse graphics by learning to generate 3D rigid objects (*e.g.* human/animal faces, CAD models) from 2D image collections. However, human bodies, as articulated objects, have complex articulations and diverse appearances. Therefore, it is challenging to learn 3D human generative models that can synthesis animatable 3D humans with high-fidelity textures and vivid geometric details.

To generate high-quality 3D humans, we argue that two main factors should be properly addressed: **1) 3D human representation**; **2) generative network training strategies**. Due to the articulated nature of human bodies, a desirable human representation should be able to explicitly control the pose/shape of 3D humans. An articulated 3D human representation need to be designed, rather than the static volume modeling utilized in existing 3D-aware GANs. With an articulated representation, a 3D human is modeled in its canonical pose (canonical space), and can be rendered in different poses and shapes (observation space). Moreover, the efficiency of the representation matters in high-quality 3D human generation. Previous methods (Noguchi et al., 2022; Bergman et al., 2022) fail to achieve high resolution generation due to their inefficient human representations.

In addition, training strategies could also highly influence 3D human generative models. The issue mainly comes from the data characteristics. Compared with datasets used by Noguchi et al. (2022) (*e.g.* AIST (Tsuchida et al., 2019)), fashion datasets (*e.g.* DeepFashion (Liu et al., 2016)) are more aligned with real-world human image distributions, making a favorable dataset choice. AIST only has 40 dancers, which are mostly dressed in black. In contrast, DeepFashion contains much more different persons wearing various clothes, which benefits the diversity and quality of 3D human generation. However, fashion datasets mostly have **very limited human poses** (most are similar standing poses), and **highly imbalanced viewing angles** (most are front views). This imbalanced 2D data distribution could hinder unsupervised learning of 3D GANs, leading to difficulties in novel view/ pose synthesis. Therefore, a proper training strategy is in need to alleviate the issue.

In this work, we propose **EVA3D**, an unconditional high-quality 3D human generative model from sparse 2D human image collections only. To facilitate that, we propose a compositional human NeRF representation to improve the model efficiency. We divide the human body into 16 parts and assign each part an individual network, which models the corresponding local volume. Our human representation mainly provides three advantages. **1)** It inherently describes the human body prior, which supports explicit control over human body shapes and poses. **2)** It supports adaptively allocating computation resources. More complex body parts (*e.g.* heads) can be allocated with more parameters. **3)** The compositional representation enables efficient rendering and achieves high-resolution generation. Rather than using one big volume (Bergman et al., 2022), our compositional representation tightly models each body part and prevents wasting parameters on empty volumes. Moreover, thanks to the part-based modeling, we can efficiently sample rays inside local volumes and avoid sampling empty spaces. With the compact representation together with the efficient rendering algorithm, we achieve high-resolution (512×256) rendering and GAN training without using super-resolution modules, while existing methods can only train at a native resolution of 128^2.

Moreover, we carefully design training strategies to address the human pose and viewing angle imbalance issue. We analyze the head-facing angle distribution and propose a pose-guided sampling strategy to help effective 3D human geometry learning. Besides, we utilize the SMPL model to leverage its human prior during training. Specifically, we use SMPL skinning weights to guide the transformation between canonical and observation spaces, which shows good robustness to the pose distribution of the dataset and brings better generalizability to novel pose generation. We further use SMPL as the geometry template and predict offsets to help better geometry learning.

Quantitative and qualitative experiments are performed on two fashion datasets (Liu et al., 2016; Fu et al., 2022) to demonstrate the advantages of EVA3D. We also experiment on UBCFashion (Zablotskaia et al., 2019) and AIST (Tsuchida et al., 2019) for comparison with prior work. Extensive experiments on our method designs are provided for further analysis. In conclusion, our contributions are as follows: **1)** We are the first to achieve high-resolution high-quality 3D human generation from 2D image collections; **2)** We propose a compositional human NeRF representation tailored for efficient GAN training; **3)** Practical training strategies are introduced to address the imbalance issue of real 2D human image collections. **4)** We demonstrate applications of EVA3D, *i.e.* interpolation and GAN inversion, which pave way for further exploration in 3D human GAN.

2 RELATED WORK

3D-Aware GAN. Generative Adversarial Network (GAN) (Goodfellow et al., 2020) has been a great success in 2D image generation (Karras et al., 2019; 2020). Many efforts have also been put on 3D-aware generation. Nguyen-Phuoc et al. (2019); Henzler et al. (2019) use voxels, and Pan et al. (2020) use meshes to assist the 3D-aware generation. With recent advances in NeRF (Mildenhall et al., 2020; Tewari et al., 2021), many have build 3D-aware GANs based on NeRF (Schwarz et al., 2020; Niemeyer & Geiger, 2021; Chan et al., 2021; Deng et al., 2022). To increase the generation resolution, Gu et al. (2021); Or-El et al. (2022); Chan et al. (2022) use 2D decoders for super resolution. Moreover, it is desirable to lift the raw resolution, by improving the rendering efficiency, for more detailed geometry and better 3D consistency (Skorokhodov et al., 2022; Xiang et al., 2022). We also propose an efficient 3D human representation to allow high resolution training.

Human Generation. Though great success has been achieved in generating human faces, it is still challenging to generate human images for the complexity in human poses and appearances (Sarkar et al., 2021b; Lewis et al., 2021; Sarkar et al., 2021a; Jiang et al., 2022c). Recently, Fu et al. (2022); Frühstück et al. (2022) scale-up the dataset and achieve impressive 2D human generation results. For 3D human generation, Chen et al. (2022) generate human geometry using 3D human dataset. Some also attempt to train 3D human GANs using only 2D human image collections. Grigorev et al. (2021); Zhang et al. (2021) use CNN-based neural renderers, which cannot guarantee 3D consistency. Noguchi et al. (2022) use human NeRF (Noguchi et al., 2021) for this task, which only trains at low resolution. Bergman et al. (2022); Zhang et al. (2022) propose to increase the resolution by super-resolution, which still fails to produce high-quality results.

3D Human Representations. 3D human representations serve as fundamental tools for human related tasks. Loper et al. (2015); Pavlakos et al. (2019b) create parametric human models, for explicit modeling of 3D humans. To model human appearances, Habermann et al. (2021); Shysheya et al. (2019); Yoon et al. (2021); Liu et al. (2021) further introduce UV maps. Parametric modeling gives robust control over the human model, but less realism. Palafox et al. (2021) use implicit functions to generate realistic 3D human body shapes. Embracing the development of NeRF, the number of works about human NeRF has also exploded (Peng et al., 2021b; Zhao et al., 2021; Peng et al., 2021a; Xu et al., 2021; Noguchi et al., 2021; Weng et al., 2022; Chen et al., 2021; Su et al., 2021; Jiang et al., 2022a;b; Wang et al., 2022). Some propose to model human body in a compositional way (Mihajlovic et al., 2022; Palafox et al., 2022; Su et al., 2022), where several submodules are used to model different body parts, and are more efficient than single-network ones.

3 METHODOLOGY

3.1 PREREQUISITES

NeRF (Mildenhall et al., 2020) is an implicit 3D representation, which is capable of photorealistic novel view synthesis. NeRF is defined as $\{\boldsymbol{c}, \sigma\} = F_\Phi(\boldsymbol{x}, \boldsymbol{d})$, where $\boldsymbol{x}$ is the query point, $\boldsymbol{d}$ is the viewing direction, $\boldsymbol{c}$ is the emitted radiance (RGB value), σ is the volume density. To get the RGB value $C(\boldsymbol{r})$ of some ray $\boldsymbol{r}(t) = \boldsymbol{o} + t\boldsymbol{d}$, namely volume rendering, we have the following formulation, $C(\boldsymbol{r}) = \int_{t_n}^{t_f} T(t)\sigma(\boldsymbol{r}(t))\boldsymbol{c}(\boldsymbol{r}(t), \boldsymbol{d})dt$, where $T(t) = \exp(-\int_{t_n}^{t} \sigma(\boldsymbol{r}(s))ds)$ is the accumulated transmittance along the ray $\boldsymbol{r}$ from t_n to t. t_n and t_f denotes the near and far bounds. To get the estimation of $C(\boldsymbol{r})$, it is discretized as

$$\hat{C}(\boldsymbol{r}) = \sum_{i=1}^{N} T_i(1 - \exp(-\sigma_i\delta_i))\boldsymbol{c}_i, \text{ where } T_i = \exp(-\sum_{j=1}^{i-1} \sigma_j\delta_j),\ \delta_i = t_{i+1} - t_i. \tag{1}$$

For better geometry, Or-El et al. (2022) propose to replace the volume density $\sigma(\boldsymbol{x})$ with SDF values $d(\boldsymbol{x})$ to explicitly define the surface. SDF can be converted to the volume density as $\sigma(\boldsymbol{x}) = \alpha^{-1}\text{sigmoid}\left(-d(\boldsymbol{x})/\alpha\right)$, where α is a learnable parameter. In later experiments, we mainly use SDF as the implicit geometry representation, which is denoted as σ for convenience.

SMPL (Loper et al., 2015), defined as $M(\boldsymbol{\beta}, \boldsymbol{\theta})$, is a parametric human model, where $\boldsymbol{\beta}, \boldsymbol{\theta}$ controls body shapes and poses. In this work, we use the Linear Blend Skinning (LBS) algorithm of SMPL for the transformation from the canonical space to observation spaces. Formally, point $\boldsymbol{x}$ in the canonical space is transformed to an observation space defined by pose $\boldsymbol{\theta}$ as

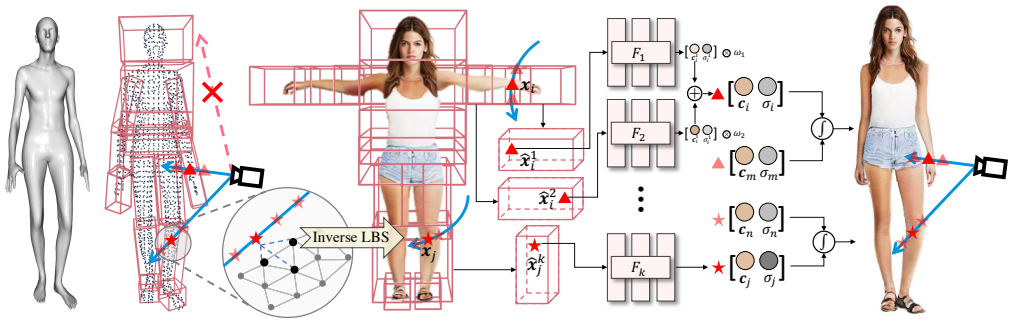

a) Sample Rays & Points at Observation Space SMPL(β, θ) **b)** Inverse LBS to Canonical Space **c)** Transform to Local Bounding Box & Query Subnetworks **d)** Integrate Queried Results Along Rays

Figure 2: **Rendering Process of the Compositional Human NeRF Representation.** For shape and pose specified by SMPL($\boldsymbol{\beta}$, $\boldsymbol{\theta}$), local bounding boxes are constructed. Rays that intersect with bounding boxes are sampled and transferred to the canonical space using inverse LBS. Subnetworks corresponding to bounding boxes are queried, results of which are integrated to produce final renderings.

$\boldsymbol{x}' = \sum_{k=1}^{K} w_k \boldsymbol{G_k}(\boldsymbol{\theta}, \boldsymbol{J})\boldsymbol{x}$, where K is the joint number, w_k is the blend weight of $\boldsymbol{x}$ against joint k, $\boldsymbol{G_k}(\boldsymbol{\theta}, \boldsymbol{J})$ is the transformation matrix of joint k. The transformation from observation spaces to the canonical space, namely inverse LBS, takes a similar formulation with inverted transformation matrices.

3.2 Compositional Human NeRF Representation

The compositional human NeRF representation is defined as $\mathbb{F}_\Phi$, corresponding to a set of local bounding boxes $\mathbb{B}$. For each body part k, we use a subnetwork $F_k \in \mathbb{F}_\Phi$ to model the local bounding box $\{\boldsymbol{b}^k_{min}, \boldsymbol{b}^k_{max}\} \in \mathbb{B}$, as shown in Fig. 2 b). For some point $\boldsymbol{x}_i$ in the canonical coordinate with direction $\boldsymbol{d}_i$ and falling inside the k-th bounding box, the corresponding radiance $\boldsymbol{c}^k_i$ and density σ^k_i is queried by

$$\{\boldsymbol{c}^k_i, \sigma^k_i\} = F_k(\hat{\boldsymbol{x}}^k_i, \boldsymbol{d}_i), \text{ where } \hat{\boldsymbol{x}}^k_i = \frac{2\boldsymbol{x}_i - (\boldsymbol{b}^k_{min} + \boldsymbol{b}^k_{max})}{\boldsymbol{b}^k_{max} - \boldsymbol{b}^k_{min}}. \tag{2}$$

If the point $\boldsymbol{x}_i$ falls in multiple bounding boxes $\mathbb{A}_i$, a window function (Lombardi et al., 2021) is applied to linearly blend queried results. The blended radiance $\boldsymbol{c}_i$ and density σ_i of $\boldsymbol{x}_i$ is calculated as

$$\{\boldsymbol{c}_i, \sigma_i\} = \frac{1}{\sum \omega_a} \sum_{a \in \mathbb{A}_i} \omega_a \{\boldsymbol{c}^k_i, \sigma^k_i\}, \text{ where } \omega_a = \exp(-m(\hat{\boldsymbol{x}}^k_i(x)^n + \hat{\boldsymbol{x}}^k_i(y)^n + \hat{\boldsymbol{x}}^k_i(z)^n)). \tag{3}$$

m, n are chosen empirically. Different from Palafox et al. (2022); Su et al. (2022), we only query subnetworks whose bounding boxes contain query points. It increases the efficiency of the query process and saves computational resources.

Taking advantages of the compositional representation, we also adopt an efficient volume rendering algorithm. Previous methods need to sample points, query, and integrate for every pixel of the canvas, which wastes large amounts of computational resources on backgrounds. In contrast, for the compositional representation, we have pre-defined bounding boxes to filter useful rays, which is also the key for our method being able to train on high resolution.

As shown in Fig. 2, for the target pose $\boldsymbol{\theta}$, shape $\boldsymbol{\beta}$ and camera setup, our rendering algorithm $\mathcal{R}(\mathbb{F}_\Phi, \boldsymbol{\beta}, \boldsymbol{\theta}, \text{cam})$ is described as follows. Firstly, ray $\boldsymbol{r}(t) = \boldsymbol{o} + t\boldsymbol{d}$ is sampled for each pixel on the canvas. Then we transform the pre-defined bounding boxes $\mathbb{B}$ to the target pose $\boldsymbol{\theta}$ using transformation matrices $\boldsymbol{G_k}$ defined by SMPL. Rays that intersect with the transformed bounding boxes are kept for further rendering. Others are marked to be the background color. For ray $\boldsymbol{r}(t) = \boldsymbol{o} + t\boldsymbol{d}$ that intersects with single or multiple bounding boxes, we get the near and far bounds t_n, t_f. N points are randomly sampled on each ray as

$$t_i \sim \mathcal{U}\left[t_n + \frac{i-1}{N}(t_f - t_n), t_n + \frac{i}{N}(t_f - t_n)\right]. \tag{4}$$

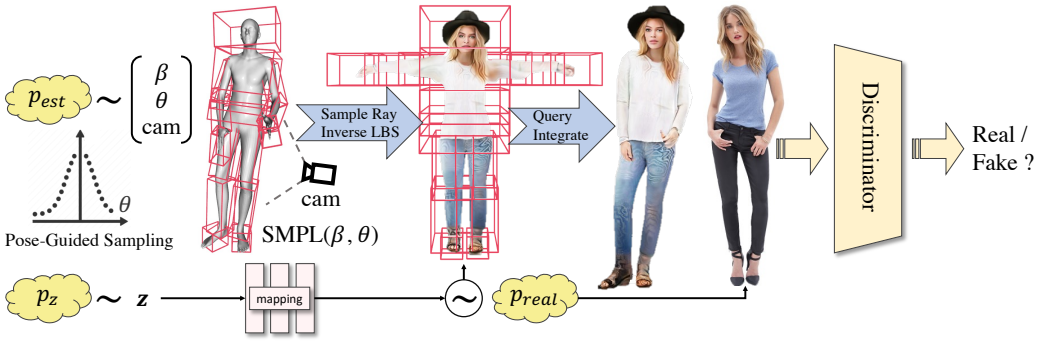

Figure 3: **3D Human GAN Framework.** With the estimated SMPL and camera parameters distribution p_{est}, 3D humans are randomly sampled and rendered conditioned on $z \sim p_z$. The renderings are used for adversarial training against real 2D human image collections p_{real}.

Next, we transform sampled points back to the canonical space using inverse LBS. Similar to Zheng et al. (2021), we inverse not only the pose transformation, but also the shape/ pose blend shapes $\boldsymbol{B_S}(\boldsymbol{\beta}), \boldsymbol{B_P}(\boldsymbol{\theta})$ to be able to generalize to different body shapes. For sampled point $\boldsymbol{r}(t_i)$, the nearest k points $\mathbb{N} = \{\boldsymbol{v}_1 ... \boldsymbol{v}_k\}$ are found among the vertices of the posed SMPL mesh $M(\boldsymbol{\beta}, \boldsymbol{\theta})$. The transformation of point $\boldsymbol{r}(t_i)$ from the observation space to the canonical space is defined as

$$\begin{bmatrix} \boldsymbol{x}_i^0 \\ \mathbf{1} \end{bmatrix} = \sum_{v_j \in \mathbb{N}} \frac{\omega_j}{\sum \omega_j} (\boldsymbol{M}_j)^{-1} \begin{bmatrix} \boldsymbol{r}(t_i) \\ \mathbf{1} \end{bmatrix}, \text{where } \boldsymbol{M}_j = \left(\sum_{k=1}^{K} w_k^j \boldsymbol{G}_k \right) \begin{bmatrix} \boldsymbol{I} & \boldsymbol{B_S^j} + \boldsymbol{B_P^j} \\ \mathbf{0} & \boldsymbol{I} \end{bmatrix}. \quad (5)$$

$\omega_j = 1/\|\boldsymbol{r}(t_i) - \boldsymbol{v_j}\|$ is the inverse distance weight. $\boldsymbol{M}_j$ is the transformation matrix of the SMPL vertex v_j. Then we query the compositional human NeRF representation $\mathbb{F}$ with point $\boldsymbol{x}_i^0$ to get its corresponding radiance $\boldsymbol{c}_i$ and density σ_i as defined in Eq. 2 and 3. Finally, we integrate the queried results for the RGB value of ray $\boldsymbol{r}(t)$, as defined in Eq. 1.

3.3 3D Human GAN Framework

With the compositional human NeRF representation, we construct a 3D human GAN framework as shown in Fig. 3. The generator is defined as $G(\boldsymbol{z}, \boldsymbol{\beta}, \boldsymbol{\theta}, \text{cam}; \Phi_G) = \mathcal{R}(\mathbb{F}_{\Phi_G}(\boldsymbol{z}), \boldsymbol{\beta}, \boldsymbol{\theta}, \text{cam})$. Similar to pi-GAN (Chan et al., 2021), each subnetwork of $\mathbb{F}_\Phi$ consists of stacked MLPs with SIREN activation (Sitzmann et al., 2020). To generate fake samples, $\boldsymbol{z} \sim p_{\boldsymbol{z}}$ is sample from normal distribution. $\{\boldsymbol{\beta}, \boldsymbol{\theta}, \text{cam}\} \sim p_{est}$ are sampled from the estimated distribution from 2D image collections. We use off-the-shelf tools (Pavlakos et al., 2019a; Kocabas et al., 2020) to estimate $\{\boldsymbol{\beta}, \boldsymbol{\theta}, \text{cam}\}$ for the 2D image collections. Unlike ENARF-GAN(Noguchi et al., 2022), where these variables are sampled from the distribution of motion datasets (Mahmood et al., 2019), the real 2D image collections do not necessarily share the similar pose distribution as that of motion datasets, especially for fashion datasets, *e.g.* DeepFashion, where the pose distribution is imbalanced. Finally, the fake samples $\boldsymbol{I}_f = G(\boldsymbol{z}, \boldsymbol{\beta}, \boldsymbol{\theta}, \text{cam}; \Phi_G)$, along with real samples $\boldsymbol{I}_r \sim p_{real}$ are sent to discriminator $D(I; \Phi_D)$ for adversarial training. For more implementation details, please refer to the supplementary material.

3.4 Training

Delta SDF Prediction. Real-world 2D human image collections, especially fashion datasets, usually have imbalanced pose distribution. For example, as shown in Fig. 6, we plot the distribution of facing angles of DeepFashion. Such heavily imbalanced pose distribution makes it hard for the network to learn correct 3D information in an unsupervised way. Therefore, we propose to introduce strong human prior by utilizing the SMPL template geometry $\boldsymbol{d}_T(\boldsymbol{x})$ as the foundation of our human representation. Instead of directly predicting the SDF value $\boldsymbol{d}(\boldsymbol{x})$, we predict an SDF offset $\Delta\boldsymbol{d}(\boldsymbol{x})$ from the template (Yifan et al., 2022). Then $\boldsymbol{d}_T(\boldsymbol{x}) + \Delta\boldsymbol{d}(\boldsymbol{x})$ is used as the actual SDF value of point $\boldsymbol{x}$.

Pose-guided Sampling. To facilitate effective 3D information learning from sparse 2D image collections, other than introducing a 3D human template, we propose to balance the input 2D images

a) Render Views Control b) Human Pose Control c) Human Shapes Control

Figure 4: **Generation Results of EVA3D.** The 3D-aware nature and inherent human prior of EVA3D enable explicit control over rendering views, human poses, and shapes.

based on human poses. The intuition behind the pose-guided sampling is that different viewing angles should be sampled more evenly to allow effective learning of geometry. Empirically, among all human joints, we use the angle of the head to guide the sampling. Moreover, facial areas contain more information than other parts of the head. Front-view angles should be sampled more than other angles. Therefore, we choose to use a Gaussian distribution centered at the front-view angle μ_θ, with a standard deviation of σ_θ. Specifically, M bins are divided on the circle. For an image with the head angle falling in bin m, its probability p_m of being sampled is defined as

$$p_m = \frac{1}{\sigma_\theta\sqrt{2\pi}}\exp\left(-\frac{1}{2}\left(\frac{\theta_m - \mu_\theta}{\sigma_\theta}\right)^2\right), \text{ where } \theta_m = \frac{2\pi m}{M}. \tag{6}$$

We visualize the balanced distribution in Fig. 6. The network now has higher chances of seeing more side-views of human bodies, which helps better geometry generation.

Loss Functions. For the adversarial training, we use the non-saturating GAN loss with R1 regularization (Mescheder et al., 2018), which is defined as

$$\mathcal{L}_{\text{adv}}(\Phi_G, \Phi_D) = \boldsymbol{E}_{\boldsymbol{z}\sim p_z, \{\boldsymbol{\beta},\boldsymbol{\theta},\text{cam}\}\sim p_{est}}[f(D(G(\boldsymbol{z}, \boldsymbol{\beta}, \boldsymbol{\theta}, \text{cam}; \Phi_G); \Phi_D))] \tag{7}$$

$$+ \boldsymbol{E}_{\boldsymbol{I}_r\sim p_{real}}[f(-D(\boldsymbol{I}_r; \Phi_D)) + \lambda|\nabla D(\boldsymbol{I}_r; \Phi_D)|^2], \tag{8}$$

where $f(u) = -\log(1 + \exp(-u))$. Other than the adversarial loss, some regularization terms are introduced for the delta SDF prediction. Firstly, we want minimum offset from the template mesh to maintain plausible human shape, which gives the minimum offset loss $\mathcal{L}_{\text{off}} = \boldsymbol{E}_{\boldsymbol{x}}[\|\Delta d(\boldsymbol{x})\|_2^2]$. Secondly, to ensure that the predicted SDF values are physically valid (Gropp et al., 2020), we penalize the derivation of delta SDF predictions to zero $\mathcal{L}_{\text{eik}} = \boldsymbol{E}_{\boldsymbol{x}}[\|\nabla(\Delta d(\boldsymbol{x}))\|_2^2]$. The overall loss is defined as $\mathcal{L} = \mathcal{L}_{\text{adv}} + \lambda_{\text{off}}\mathcal{L}_{\text{off}} + \lambda_{\text{eik}}\mathcal{L}_{\text{eik}}$, where λ_* are loss weights defined empirically.

4 Experiments

4.1 Experimental Setup

Datasets. We conduct experiments on four datasets: DeepFashion (Liu et al., 2016), SHHQ (Fu et al., 2022), UBCFashion (Zablotskaia et al., 2019) and AIST (Tsuchida et al., 2019). The first two are sparse 2D image collections, meaning that each image has different identities and poses are sparse, which makes them more challenging. The last two are human video datasets containing different poses/ views of the same identities, which is easier for the task but lacks diversity.

Comparison Methods. We mainly compare with three baselines. ENARF-GAN (Noguchi et al., 2022) makes the first attempt at human NeRF generation from 2D image collections. EG3D (Chan et al., 2022) and StyleSDF (Or-El et al., 2022) are state-of-the-art methods for 3D-aware generation, both requiring super-resolution modules to achieve high-resolution generation.

a) EG3D b) StyleSDF c) ENARF-GAN d) Ours

Figure 5: **Qualitative Comparison Between EVA3D and Baseline Methods.** Rendered 2D images and corresponding meshes are placed side-by-side. Both the 2D renderings and 3D meshes generated by our method achieve the best quality among SOTA methods. Zoom in for the best view.

Evaluation Metrics. To evaluate the quality of rendered images, we adopt Frechet Inception Distance (FID) (Heusel et al., 2017) and Kernel Inception Distance (KID) (Bińkowski et al., 2018). Following ENARF-GAN, we use Percentage of Correct Keypoints (PCKh@0.5) (Andriluka et al., 2014) to evaluate the correctness of generated poses. Note that PCKh@0.5 can only be calculated on methods that can control generated poses, *i.e.* ENARF-GAN and EVA3D. To evaluate the correctness of geometry, we use an off-the-shelf tool (Ranftl et al., 2022) to estimate depth from the generated images and compare it with generated depths. $50K$ samples padded to square are used to compute FID and KID. PCKh@0.5 and Depth are evaluated on $5K$ samples.

4.2 Qualitative Evaluations

Generation Results and Controlling Ability of EVA3D. As shown in Fig. 4 a), EVA3D is capable of generating high-quality renderings in novel views and remain multi-view consistency. Due to the inherent human prior in our model design, EVA3D can control poses and shapes of the generated 3D human by changing $\boldsymbol{\beta}$ and $\boldsymbol{\theta}$ of SMPL. We show novel pose and shape generation results in Fig. 4 b)& c). We refer readers to the supplementary PDF and video for more qualitative results.

Comparison with Baseline Methods. We show the renderings and corresponding meshes generated by baselines and our method in Fig. 5. EG3D trained on DeepFashion, as well as StyleSDF trained on SHHQ, generate reasonable RGB renderings and geometry. However, without explicit human modeling, complex human poses make it hard to align and model 3D humans in observation spaces, which leads to distorted generation. Moreover, because of the use of super resolution, their geometry is only trained under low resolution (64^2) and therefore lacks details. EG3D trained on SHHQ and StyleSDF trained on DeepFashion fail to capture 3D information and collapse to the trivial solution of painting on billboards. Limited by the inefficient representation and computational resources,

Table 1: Comparison with State-of-the-Art Methods. * The training code of ENARF-GAN is implemented based on the official inference code.

Methods, Resolution	*DeepFashion*				*SHHQ*			
	FID↓	KID↓	PCK↑	Depth↓	FID↓	KID↓	PCK↑	Depth↓
EG3D, 512^2	26.38	0.014	-	0.0779	32.96	0.033	-	0.0296
StyleSDF, 512^2	92.40	0.136	-	0.0359	14.12	0.010	-	0.0300
ENARF-GAN*, 128^2	77.03	0.114	43.74	0.1151	80.54	0.102	40.17	0.1241
Ours, 512^2	**15.91**	**0.011**	**87.50**	**0.0272**	**11.99**	**0.009**	**88.95**	**0.0177**
Methods, Resolution	*UBCFashion*				*AIST*			
	FID↓	KID↓	PCK↑	Depth↓	FID↓	KID↓	PCK↑	Depth↓
EG3D, 512^2	23.95	**0.009**	-	0.1163	34.76	0.022	-	0.1165
StyleSDF, 512^2	18.52	0.011	-	0.0311	199.5	0.225	-	0.0236
ENARF-GAN*, 128^2	-	-	-	-	73.07	0.075	42.85	0.1128
Ours, 512^2	**12.61**	0.010	**99.17**	**0.0090**	**19.40**	**0.010**	**83.15**	**0.0126**

Table 2: Results of Ablation Study. †Depth is evaluated against SMPL depth. We report †Depth$\times 10^3$ for simplicity.

Methods	FID↓	†Depth↓
Baseline, 256^2	31.14	3.57
+ Composite, 512^2	17.81	5.02
+ Delta SDF, 512^2	**15.62**	3.69
+ Pose-guide, 512^2	15.91	**3.04**

Table 3: Trade-Off Between RGB and Geometry.

Distribution	FID↓	†Depth↓
Original	15.62	3.69
$\sigma_\theta = 15°$	15.91	3.04
$\sigma_\theta = 30°$	19.05	2.58
$\sigma_\theta = 45°$	19.56	2.65
$\sigma_\theta = 60°$	25.08	2.91
Uniform	25.82	2.92

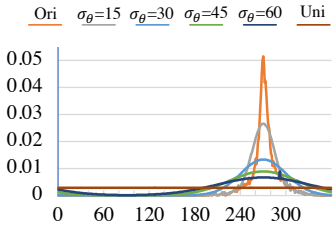

Figure 6: PDF of Different Pose-Guided Sampling Distributions.

ENARF-GAN can only be trained at a resolution of 128^2, which leads to low-quality rendering results. Besides, lacking human prior makes ENARF-GAN hard to capture correct 3D information of human from sparse 2D image collections, which results in broken meshes. EVA3D, in contrast, generates high-quality human renderings on both datasets. We also succeeded in learning reasonable 3D human geometry from 2D image collections with sparse viewing angles and poses, thanks to the strong human prior and the pose-guided sampling strategy. Due to space limitations, we only show results of DeepFashion and SHHQ here. For visual comparisons on UBCFashion and AIST, please refer to the supplementary material.

4.3 Quantitative Evaluations

As shown in Tab. 1, our method leads all metrics in four datasets. EVA3D outperforms ENARF-GAN in all settings thanks to our high-resolution training ability. EG3D and StyleSDF, as the SOTA methods in the 3D generation, can achieve reasonable scores in some settings (*e.g.* StyleSDF achieves 18.52 FID on UBCFashion) for their super-resolution modules. But they also fail on some datasets (*e.g.* StyleSDF fails on AIST with 199.5 FID) for complexity in human poses. In the contrast, EVA3D achieves the best FID/KID scores under all settings. Moreover, unlike EG3D or StyleSDF, EVA3D can control the generated pose and achieve higher PCKh@0.5 score than ENARF-GAN. For the geometry part, we also achieve the lowest depth error, which shows the importance of natively high-resolution training.

4.4 Ablation Studies

Ablation on Method Designs. To validate the effectiveness of our designs on EVA3D, we subsequently add different designs on a baseline method, which uses one large network to model the canonical space. Experiments are conducted on DeepFashion. The results are reported in Tab. 2. Limited by the inefficient representation, the baseline ("Baseline") can only be trained at 256×128, which results in the worst FID score. Adding compositional design ("+Composite") makes the network efficient enough to be trained at a higher resolution of 512×256 and achieve higher generation quality. We further introduce human prior by predicting delta SDF ("+Delta SDF"), which gives the best FID score and lower depth error. Finally, using the pose-guided sampling ("+Pose-guide"),

Figure 7: **Applications of EVA3D.** a) Interpolation on the latent space gives smooth transition between two samples. b) Inversion results (right) of the target image (left).

we further decrease the depth error, which means better geometry. However, the FID score slightly increases, which is discussed in the next paragraph. We refer readers to the supplementary material for qualitative evaluations of ablation studies.

Analysis on Pose-Guided Sampling. We further analyze the importance of the sampling strategy in 3D human GAN training. Three types of distributions p_{est} are experimented, including the original dataset distribution ("Original"), pose-guided Gaussian distribution ("$\sigma_\theta = *$"), and pose-guided uniform distribution ("Uniform"). The results are reported in Tab. 3. Firstly, uniform sampling is not a good strategy, as shown by its high FID score. This is because the information density is different between different parts of human. Faces require more training iterations. Secondly, the original distribution gives the best visual quality but the worst geometry. As shown in Fig. 6, the original distribution leads to the network mostly being trained on front-view images. It could result in the trivial solution of painting on billboards. Though using delta SDF prediction can alleviate the problem to some extent, the geometry is still not good enough. Thirdly, the pose-guided Gaussian sampling can avoid damaging visual quality too much and improve geometry learning. As the standard deviation σ_θ increases, FID increases while the depth error decreases. Therefore, it is a trade-off between visual quality and geometry quality. In our final experiments, we choose $\sigma_\theta = 15^\circ$ which is a satisfying balance between the two factors.

4.5 Applications

Interpolation on Latent Space. As shown in Fig. 7 a), we linearly interpolate two latent codes to generate a smooth transition between them, showing that the latent space learned by EVA3D is semantically meaningful. More results are provided in the supplementary video.

Inversion. We use Pivotal Tuning Inversion (PTI) (Roich et al., 2021) to inverse the target image and show the results in Fig. 7 b). Reasonable novel view synthesis results can be achieved. The geometry, however, fails to capture geometry details corresponding to RGB renderings, which can be caused by the second stage generator fine-tuning of PTI. Nevertheless, we demonstrate the potential of EVA3D in more related downstream tasks.

5 Discussion

To conclude, we propose a high-quality unconditional 3D human generation model EVA3D that only requires 2D image collections for training. We design a compositional human NeRF representation for efficient GAN training. To train on the challenging 2D image collections with sparse viewing angles and human poses, *e.g.* DeepFashion, strong human prior and pose-guided sampling are introduced for better GAN learning. On four large-scale 2D human datasets, we achieve state-of-the-art generation results at a high resolution of 512×256.

Limitations: 1) There still exists visible circular artifacts in the renderings, which might be caused by the SIREN activation. A better base representation, *e.g.* tri-plane of EG3D, and a 2D decoder might solve the issue. **2)** The estimation of SMPL parameters from 2D image collections is not accurate, which leads to a distribution shift from the real pose distribution and possibly compromises generation results. Refining SMPL estimation during training would make a good future work. **3)** Limited by our tight 3D human representation, it is hard to model loose clothes like dresses. Using separate modules to handle loose clothes might be a promising direction.

ETHICS STATEMENT

Although the results of EVA3D are yet to the point where they can fake human eyes, we still need to be aware of its potential ethical issues. The generated 3D humans might be misused to create contents that are misleading. EVA3D can also be used to invert real human images, which can be used to create fake videos of real humans and cause negative social impacts. Moreover, the generated 3D humans might be biased, which is caused by the inherent distribution of training datasets. We make our best effort to demonstrate the impartiality of EVA3D in Fig. 1.

REPRODUCIBILITY STATEMENT

Our method is thoroughly described in Sec. 3. Together with implementation details included in the supplementary material, the reproducibility is ensured. Moreover, our code will be released upon acceptance.

REFERENCES

Mykhaylo Andriluka, Leonid Pishchulin, Peter Gehler, and Bernt Schiele. 2d human pose estimation: New benchmark and state of the art analysis. In *Proceedings of the IEEE Conference on computer Vision and Pattern Recognition*, pp. 3686–3693, 2014.

Alexander W Bergman, Petr Kellnhofer, Yifan Wang, Eric R Chan, David B Lindell, and Gordon Wetzstein. Generative neural articulated radiance fields. *arXiv preprint arXiv:2206.14314*, 2022.

Mikołaj Bińkowski, Danica J Sutherland, Michael Arbel, and Arthur Gretton. Demystifying mmd gans. *arXiv preprint arXiv:1801.01401*, 2018.

Eric R Chan, Marco Monteiro, Petr Kellnhofer, Jiajun Wu, and Gordon Wetzstein. pi-gan: Periodic implicit generative adversarial networks for 3d-aware image synthesis. In *Proceedings of the IEEE/CVF conference on computer vision and pattern recognition*, pp. 5799–5809, 2021.

Eric R Chan, Connor Z Lin, Matthew A Chan, Koki Nagano, Boxiao Pan, Shalini De Mello, Orazio Gallo, Leonidas J Guibas, Jonathan Tremblay, Sameh Khamis, et al. Efficient geometry-aware 3d generative adversarial networks. In *Proceedings of the IEEE/CVF Conference on Computer Vision and Pattern Recognition*, pp. 16123–16133, 2022.

Jianchuan Chen, Ying Zhang, Di Kang, Xuefei Zhe, Linchao Bao, Xu Jia, and Huchuan Lu. Animatable neural radiance fields from monocular rgb videos. *arXiv preprint arXiv:2106.13629*, 2021.

Xu Chen, Tianjian Jiang, Jie Song, Jinlong Yang, Michael J Black, Andreas Geiger, and Otmar Hilliges. gdna: Towards generative detailed neural avatars. *arXiv*, 2022.

Yu Deng, Jiaolong Yang, Jianfeng Xiang, and Xin Tong. Gram: Generative radiance manifolds for 3d-aware image generation. In *Proceedings of the IEEE/CVF Conference on Computer Vision and Pattern Recognition (CVPR)*, pp. 10673–10683, June 2022.

Anna Frühstück, Krishna Kumar Singh, Eli Shechtman, Niloy J Mitra, Peter Wonka, and Jingwan Lu. Insetgan for full-body image generation. In *Proceedings of the IEEE/CVF Conference on Computer Vision and Pattern Recognition*, pp. 7723–7732, 2022.

Jianglin Fu, Shikai Li, Yuming Jiang, Kwan-Yee Lin, Chen Qian, Chen Change Loy, Wayne Wu, and Ziwei Liu. Stylegan-human: A data-centric odyssey of human generation. *arXiv preprint arXiv:2204.11823*, 2022.

Ian Goodfellow, Jean Pouget-Abadie, Mehdi Mirza, Bing Xu, David Warde-Farley, Sherjil Ozair, Aaron Courville, and Yoshua Bengio. Generative adversarial networks. *Communications of the ACM*, 63(11):139–144, 2020.

Artur Grigorev, Karim Iskakov, Anastasia Ianina, Renat Bashirov, Ilya Zakharkin, Alexander Vakhitov, and Victor Lempitsky. Stylepeople: A generative model of fullbody human avatars. In *Proceedings of the IEEE/CVF Conference on Computer Vision and Pattern Recognition*, pp. 5151–5160, 2021.

Amos Gropp, Lior Yariv, Niv Haim, Matan Atzmon, and Yaron Lipman. Implicit geometric regularization for learning shapes. *arXiv preprint arXiv:2002.10099*, 2020.

Jiatao Gu, Lingjie Liu, Peng Wang, and Christian Theobalt. Stylenerf: A style-based 3d-aware generator for high-resolution image synthesis. *arXiv preprint arXiv:2110.08985*, 2021.

Marc Habermann, Lingjie Liu, Weipeng Xu, Michael Zollhoefer, Gerard Pons-Moll, and Christian Theobalt. Real-time deep dynamic characters. *ACM Transactions on Graphics (TOG)*, 40(4): 1–16, 2021.

Philipp Henzler, Niloy J Mitra, and Tobias Ritschel. Escaping plato's cave: 3d shape from adversarial rendering. In *Proceedings of the IEEE/CVF International Conference on Computer Vision*, pp. 9984–9993, 2019.

Martin Heusel, Hubert Ramsauer, Thomas Unterthiner, Bernhard Nessler, and Sepp Hochreiter. Gans trained by a two time-scale update rule converge to a local nash equilibrium. *Advances in neural information processing systems*, 30, 2017.

Boyi Jiang, Yang Hong, Hujun Bao, and Juyong Zhang. Selfrecon: Self reconstruction your digital avatar from monocular video. In *Proceedings of the IEEE/CVF Conference on Computer Vision and Pattern Recognition*, pp. 5605–5615, 2022a.

Wei Jiang, Kwang Moo Yi, Golnoosh Samei, Oncel Tuzel, and Anurag Ranjan. Neuman: Neural human radiance field from a single video. *arXiv preprint arXiv:2203.12575*, 2022b.

Yuming Jiang, Shuai Yang, Haonan Qiu, Wayne Wu, Chen Change Loy, and Ziwei Liu. Text2human: Text-driven controllable human image generation. *ACM Transactions on Graphics (TOG)*, 41(4):1–11, 2022c. doi: 10.1145/3528223.3530104.

Tero Karras, Samuli Laine, and Timo Aila. A style-based generator architecture for generative adversarial networks. In *Proceedings of the IEEE/CVF conference on computer vision and pattern recognition*, pp. 4401–4410, 2019.

Tero Karras, Samuli Laine, Miika Aittala, Janne Hellsten, Jaakko Lehtinen, and Timo Aila. Analyzing and improving the image quality of stylegan. In *Proceedings of the IEEE/CVF conference on computer vision and pattern recognition*, pp. 8110–8119, 2020.

Muhammed Kocabas, Nikos Athanasiou, and Michael J Black. Vibe: Video inference for human body pose and shape estimation. In *Proceedings of the IEEE/CVF conference on computer vision and pattern recognition*, pp. 5253–5263, 2020.

Kathleen M Lewis, Srivatsan Varadharajan, and Ira Kemelmacher-Shlizerman. Tryongan: Body-aware try-on via layered interpolation. *ACM Transactions on Graphics (TOG)*, 40(4):1–10, 2021.

Lingjie Liu, Marc Habermann, Viktor Rudnev, Kripasindhu Sarkar, Jiatao Gu, and Christian Theobalt. Neural actor: Neural free-view synthesis of human actors with pose control. *ACM Transactions on Graphics (TOG)*, 40(6):1–16, 2021.

Ziwei Liu, Ping Luo, Shi Qiu, Xiaogang Wang, and Xiaoou Tang. Deepfashion: Powering robust clothes recognition and retrieval with rich annotations. In *Proceedings of IEEE Conference on Computer Vision and Pattern Recognition (CVPR)*, June 2016.

Stephen Lombardi, Tomas Simon, Gabriel Schwartz, Michael Zollhoefer, Yaser Sheikh, and Jason Saragih. Mixture of volumetric primitives for efficient neural rendering. *ACM Transactions on Graphics (TOG)*, 40(4):1–13, 2021.

Matthew Loper, Naureen Mahmood, Javier Romero, Gerard Pons-Moll, and Michael J Black. Smpl: A skinned multi-person linear model. *ACM transactions on graphics (TOG)*, 34(6):1–16, 2015.

Naureen Mahmood, Nima Ghorbani, Nikolaus F Troje, Gerard Pons-Moll, and Michael J Black. Amass: Archive of motion capture as surface shapes. In *Proceedings of the IEEE/CVF international conference on computer vision*, pp. 5442–5451, 2019.

Lars Mescheder, Andreas Geiger, and Sebastian Nowozin. Which training methods for gans do actually converge? In *International conference on machine learning*, pp. 3481–3490. PMLR, 2018.

Marko Mihajlovic, Shunsuke Saito, Aayush Bansal, Michael Zollhoefer, and Siyu Tang. Coap: Compositional articulated occupancy of people. In *Proceedings of the IEEE/CVF Conference on Computer Vision and Pattern Recognition*, pp. 13201–13210, 2022.

Ben Mildenhall, Pratul P Srinivasan, Matthew Tancik, Jonathan T Barron, Ravi Ramamoorthi, and Ren Ng. Nerf: Representing scenes as neural radiance fields for view synthesis. In *European conference on computer vision*, pp. 405–421. Springer, 2020.

Thu Nguyen-Phuoc, Chuan Li, Lucas Theis, Christian Richardt, and Yong-Liang Yang. Hologan: Unsupervised learning of 3d representations from natural images. In *Proceedings of the IEEE/CVF International Conference on Computer Vision*, pp. 7588–7597, 2019.

Michael Niemeyer and Andreas Geiger. Giraffe: Representing scenes as compositional generative neural feature fields. In *Proceedings of the IEEE/CVF Conference on Computer Vision and Pattern Recognition*, pp. 11453–11464, 2021.

Atsuhiro Noguchi, Xiao Sun, Stephen Lin, and Tatsuya Harada. Neural articulated radiance field. In *Proceedings of the IEEE/CVF International Conference on Computer Vision*, pp. 5762–5772, 2021.

Atsuhiro Noguchi, Xiao Sun, Stephen Lin, and Tatsuya Harada. Unsupervised learning of efficient geometry-aware neural articulated representations. *arXiv preprint arXiv:2204.08839*, 2022.

Roy Or-El, Xuan Luo, Mengyi Shan, Eli Shechtman, Jeong Joon Park, and Ira Kemelmacher-Shlizerman. Stylesdf: High-resolution 3d-consistent image and geometry generation. In *Proceedings of the IEEE/CVF Conference on Computer Vision and Pattern Recognition*, pp. 13503–13513, 2022.

Pablo Palafox, Aljaž Božič, Justus Thies, Matthias Nießner, and Angela Dai. Npms: Neural parametric models for 3d deformable shapes. *arXiv preprint arXiv:2104.00702*, 2021.

Pablo Palafox, Nikolaos Sarafianos, Tony Tung, and Angela Dai. Spams: Structured implicit parametric models. In *Proceedings of the IEEE/CVF Conference on Computer Vision and Pattern Recognition*, pp. 12851–12860, 2022.

Xingang Pan, Bo Dai, Ziwei Liu, Chen Change Loy, and Ping Luo. Do 2d gans know 3d shape? unsupervised 3d shape reconstruction from 2d image gans. *arXiv preprint arXiv:2011.00844*, 2020.

Georgios Pavlakos, Vasileios Choutas, Nima Ghorbani, Timo Bolkart, Ahmed AA Osman, Dimitrios Tzionas, and Michael J Black. Expressive body capture: 3d hands, face, and body from a single image. In *Proceedings of the IEEE/CVF conference on computer vision and pattern recognition*, pp. 10975–10985, 2019a.

Georgios Pavlakos, Vasileios Choutas, Nima Ghorbani, Timo Bolkart, Ahmed AA Osman, Dimitrios Tzionas, and Michael J Black. Expressive body capture: 3d hands, face, and body from a single image. In *Proceedings of the IEEE/CVF Conference on Computer Vision and Pattern Recognition*, pp. 10975–10985, 2019b.

Sida Peng, Junting Dong, Qianqian Wang, Shangzhan Zhang, Qing Shuai, Hujun Bao, and Xiaowei Zhou. Animatable neural radiance fields for human body modeling. *arXiv e-prints*, pp. arXiv–2105, 2021a.

Sida Peng, Yuanqing Zhang, Yinghao Xu, Qianqian Wang, Qing Shuai, Hujun Bao, and Xiaowei Zhou. Neural body: Implicit neural representations with structured latent codes for novel view synthesis of dynamic humans. In *Proceedings of the IEEE/CVF Conference on Computer Vision and Pattern Recognition*, pp. 9054–9063, 2021b.

René Ranftl, Katrin Lasinger, David Hafner, Konrad Schindler, and Vladlen Koltun. Towards robust monocular depth estimation: Mixing datasets for zero-shot cross-dataset transfer. *IEEE Transactions on Pattern Analysis and Machine Intelligence*, 44(3), 2022.

Daniel Roich, Ron Mokady, Amit H Bermano, and Daniel Cohen-Or. Pivotal tuning for latent-based editing of real images. *arXiv preprint arXiv:2106.05744*, 2021.

Kripasindhu Sarkar, Vladislav Golyanik, Lingjie Liu, and Christian Theobalt. Style and pose control for image synthesis of humans from a single monocular view. *arXiv preprint arXiv:2102.11263*, 2021a.

Kripasindhu Sarkar, Lingjie Liu, Vladislav Golyanik, and Christian Theobalt. Humangan: A generative model of humans images. *arXiv preprint arXiv:2103.06902*, 2021b.

Katja Schwarz, Yiyi Liao, Michael Niemeyer, and Andreas Geiger. Graf: Generative radiance fields for 3d-aware image synthesis. *Advances in Neural Information Processing Systems*, 33:20154–20166, 2020.

Aliaksandra Shysheya, Egor Zakharov, Kara-Ali Aliev, Renat Bashirov, Egor Burkov, Karim Iskakov, Aleksei Ivakhnenko, Yury Malkov, Igor Pasechnik, Dmitry Ulyanov, et al. Textured neural avatars. In *Proceedings of the IEEE/CVF Conference on Computer Vision and Pattern Recognition*, pp. 2387–2397, 2019.

Vincent Sitzmann, Julien Martel, Alexander Bergman, David Lindell, and Gordon Wetzstein. Implicit neural representations with periodic activation functions. *Advances in Neural Information Processing Systems*, 33:7462–7473, 2020.

Ivan Skorokhodov, Sergey Tulyakov, Yiqun Wang, and Peter Wonka. Epigraf: Rethinking training of 3d gans. *arXiv preprint arXiv:2206.10535*, 2022.

Shih-Yang Su, Frank Yu, Michael Zollhöfer, and Helge Rhodin. A-nerf: Articulated neural radiance fields for learning human shape, appearance, and pose. *Advances in Neural Information Processing Systems*, 34:12278–12291, 2021.

Shih-Yang Su, Timur Bagautdinov, and Helge Rhodin. Danbo: Disentangled articulated neural body representations via graph neural networks. *arXiv preprint arXiv:2205.01666*, 2022.

Ayush Tewari, Justus Thies, Ben Mildenhall, Pratul Srinivasan, Edgar Tretschk, Yifan Wang, Christoph Lassner, Vincent Sitzmann, Ricardo Martin-Brualla, Stephen Lombardi, et al. Advances in neural rendering. *arXiv preprint arXiv:2111.05849*, 2021.

Shuhei Tsuchida, Satoru Fukayama, Masahiro Hamasaki, and Masataka Goto. Aist dance video database: Multi-genre, multi-dancer, and multi-camera database for dance information processing. In *Proceedings of the 20th International Society for Music Information Retrieval Conference, ISMIR 2019*, pp. 501–510, Delft, Netherlands, November 2019.

Shaofei Wang, Katja Schwarz, Andreas Geiger, and Siyu Tang. Arah: Animatable volume rendering of articulated human sdfs. In *European conference on computer vision*, volume 4, 2022.

Chung-Yi Weng, Brian Curless, Pratul P Srinivasan, Jonathan T Barron, and Ira Kemelmacher-Shlizerman. Humannerf: Free-viewpoint rendering of moving people from monocular video. In *Proceedings of the IEEE/CVF Conference on Computer Vision and Pattern Recognition*, pp. 16210–16220, 2022.

Jianfeng Xiang, Jiaolong Yang, Yu Deng, and Xin Tong. Gram-hd: 3d-consistent image generation at high resolution with generative radiance manifolds. *arXiv preprint arXiv:2206.07255*, 2022.

Hongyi Xu, Thiemo Alldieck, and Cristian Sminchisescu. H-nerf: Neural radiance fields for rendering and temporal reconstruction of humans in motion. *Advances in Neural Information Processing Systems*, 34, 2021.

Wang Yifan, Lukas Rahmann, and Olga Sorkine-hornung. Geometry-consistent neural shape representation with implicit displacement fields. In *International Conference on Learning Representations*, 2022. URL `https://openreview.net/forum?id=yhCp5RcZD7`.

Jae Shin Yoon, Lingjie Liu, Vladislav Golyanik, Kripasindhu Sarkar, Hyun Soo Park, and Christian Theobalt. Pose-guided human animation from a single image in the wild. In *Proceedings of the IEEE/CVF Conference on Computer Vision and Pattern Recognition*, pp. 15039–15048, 2021.

Polina Zablotskaia, Aliaksandr Siarohin, Bo Zhao, and Leonid Sigal. Dwnet: Dense warp-based network for pose-guided human video generation. *arXiv preprint arXiv:1910.09139*, 2019.

Jianfeng Zhang, Zihang Jiang, Dingdong Yang, Hongyi Xu, Yichun Shi, Guoxian Song, Zhongcong Xu, Xinchao Wang, and Jiashi Feng. Avatargen: a 3d generative model for animatable human avatars. *arXiv preprint arXiv:2208.00561*, 2022.

Jichao Zhang, Enver Sangineto, Hao Tang, Aliaksandr Siarohin, Zhun Zhong, Nicu Sebe, and Wei Wang. 3d-aware semantic-guided generative model for human synthesis. *arXiv preprint arXiv:2112.01422*, 2021.

Fuqiang Zhao, Wei Yang, Jiakai Zhang, Pei Lin, Yingliang Zhang, Jingyi Yu, and Lan Xu. Humannerf: Generalizable neural human radiance field from sparse inputs. *arXiv preprint arXiv:2112.02789*, 2021.

Zerong Zheng, Tao Yu, Yebin Liu, and Qionghai Dai. Pamir: Parametric model-conditioned implicit representation for image-based human reconstruction. *IEEE transactions on pattern analysis and machine intelligence*, 44(6):3170–3184, 2021.